

Generalized quantum measurement in spin-correlated hyperon-antihyperon decays

Sihao Wu,^{1,*} Chen Qian,^{2,†} Yang-Guang Yang,³ and Qun Wang^{1,4}

¹*Department of Modern Physics, University of Science and Technology of China, Hefei 230026, China*

²*Beijing Academy of Quantum Information Sciences, Beijing 100193, China*

³*Institute of Modern Physics, Chinese Academy of Sciences, Lanzhou 730000, China*

⁴*School of Mechanics and Physics, Anhui University of Science and Technology, Huainan, Anhui 232001, China*

The rapid developments of Quantum Information Science (QIS) have opened up new avenues for exploring fundamental physics. Quantum nonlocality, a key aspect for distinguishing quantum information from classical one, has undergone extensive examinations in particles' decays through the violation of Bell-type inequalities. Despite these advancements, a comprehensive framework based on quantum information theory for particle interaction is still lacking. Trying to close this gap, we introduce a generalized quantum measurement description for decay processes of spin-1/2 hyperons. We validate this approach by aligning it with established theoretical calculations and apply it to the joint decay of correlated $\Lambda\bar{\Lambda}$ pairs. We employ quantum simulation to observe the violation of CHSH inequalities in hyperon decays. Our generalized measurement description is adaptable and can be extended to a variety of high energy processes, including decays of vector mesons, $J/\psi, \psi(2S) \rightarrow \Lambda\bar{\Lambda}$, in the Beijing Spectrometer III (BESIII) experiment at the Beijing Electron Positron Collider (BEPC). The methodology developed in this study can be applied to quantum correlation and information processing in fundamental interactions.

I. INTRODUCTION

Quantum field theory based on quantum mechanics and special relativity is an underlying theory for elementary particles and their interactions. Quantum information theory can offer us a new perspective for the study of elementary particles and their interactions [1, 2]. An essential feature of quantum mechanics is quantum nonlocality characterized by the violation of Bell-type inequalities [3–5]. Previously, these Bell-type inequalities have been widely applied in photonic and atomic systems detecting quantum correlation of electromagnetic interaction at low energy [6, 7]. High-energy processes also provide an alternative testing ground for quantum nonlocality in electroweak and strong interactions [8, 9] with increasingly precise data. Recently there are a lot of works that have been done along this line in different particle systems, e.g., the hyperon-antihyperon system in charmonium decays at Beijing Electron Positron Collider (BEPC) [10–16], the Λ hyperon pairs in string fragmentation [17], the top quark and anti-top quark ($t\bar{t}$) system produced at Large Hadron Collider (LHC) [1, 18–21], the leptons pairs from e^+e^- annihilation or Higgs decay [22], and correlated vector bosons and Higgs bosons in high energy processes [23–26]. It is worth mentioning that the quantum entanglement in string fragmentation in high energy processes such as electron-positron and electron-proton collisions can be studied using the spin correlation of the hyperon-antihyperon system [17, 27]. The spin correlation of the hyperon-antihyperon system has also been studied in heavy-ion collisions and can provide information on the vorticity structure of the strong interaction matter [28, 29].

However, there are still some difficulties in testing Bell-type inequalities in particle physics. One difficulty is that it is hard to overcome all loopholes especially in high energy interactions [30]. Another is that we would encounter different Bell-type inequalities in different particle decays because decay parameters vary for different particles, which seems to lack a general feature [11, 12, 14]. For these reasons, we need to search for a general framework to describe quantum properties in high energy processes with the help of quantum information theory. Recently the decay processes of particles have been characterized as quantum measurement processes [11, 12] with particle interactions interpreted as quantum channels [2]. Moreover, quantum tomography has been employed to analyze quantum correlation in top-antitop quark pairs [1, 18, 21]. Despite these works, a general framework for particle interactions in the viewpoint of quantum information theory has yet to be established.

The purpose of this paper is to explore a mapping between the generalized quantum measurement and the particle decay process. We will focus on decays of spin-1/2 hyperons, especially $\Lambda\bar{\Lambda}$ hyperon pair from decays of spin-0 charmonia η_c and χ_{c0} . We describe decay processes of spin-1/2 hyperons in the language of generalized quantum measurement and quantum channel. The generalized measurement in Bloch-Fano representation is also introduced for decay processes. Then we apply the method to study the quantum correlation in $\Lambda\bar{\Lambda}$ from decays of η_c and χ_{c0} . Finally, we perform the quantum simulation to test the CHSH inequality in $\Lambda\bar{\Lambda}$ and their decay daughters on the quantum computing platform *Quafu*.

The paper is organized as follows. We briefly review the concept of the generalized quantum measurement and decay parameters of spin-1/2 hyperons in Sec. II, and then describe decay processes of spin-1/2 hyperons in the framework of the generalized measurement and quantum

* shwu@mail.ustc.edu.cn

† qianchen@baqis.ac.cn

channel in Sec. III and Sec. IV, respectively. We perform the quantum simulation to test the CHSH inequality in Sec. V. We have a discussion about the connection between the quantum measurement and particle reaction processes in Sec. VI. A summary of the main result and outlook is given in Sec. VII.

II. PRELIMINARIES

In this section, we briefly review some concepts in quantum measurement theory and hyperon decays, which will be used in the following sections.

A. Generalized measurement and quantum channel

In Quantum Information Science (QIS), the measurement postulate is employed to describe the act of measurement on a quantum system [31]. According to this postulate, the measurement processes in quantum physics are subjected by a collection of *measurement operators* $\{M_m\}$. These processes are defined as *generalized measurements*, distinguishing from the well-known *projective measurements* or *von Neumann measurements*, which have to be orthogonal. When we use the density operator ρ to describe a system being measured, the probability of obtaining a certain outcome m is given by

$$\mathcal{P}(m) = \text{Tr}(M_m \rho M_m^\dagger), \quad (1)$$

where $\{\mathcal{P}(m)\}$ are probability distributions for all possible outcomes satisfying the non-negative condition $\mathcal{P}(m) \geq 0$ and the normalization condition $\sum_m \mathcal{P}(m) = 1$. These two conditions lead to constraints on $\{M_m\}$: the positive semidefiniteness: $M_m^\dagger M_m \geq 0$, and the completeness: $\sum_m M_m^\dagger M_m = \mathbb{1}$. Based on the measurement postulate in quantum mechanics, the initial state ρ instantaneously transforms after the measurement to the state ρ_m ,

$$\rho \mapsto \rho_m = \frac{M_m \rho M_m^\dagger}{\mathcal{P}(m)}, \quad (2)$$

where the subscript of ρ_m corresponds to the outcome m . One can also define the *positive operator-valued measurement* (POVM) [31] through the generalized measurement as $F_m \equiv M_m^\dagger M_m$ with the probability $\mathcal{P}(m) = \text{Tr}(F_m \rho)$ following Eq. (1). The POVM formalism has been used in some recent works in high energy physics [26].

Nevertheless, sometimes we cannot accurately obtain measurement outcomes in real experiments. That is, if we lose the track of some measurement outcomes, the resulting quantum states are described by an ensemble $\{\mathcal{P}(m), \rho_m\}$, which indicates that the post-measurement state ρ_m has the probability $\mathcal{P}(m)$. The

post-measurement state is then

$$\begin{aligned} \sum_m \mathcal{P}(m) \rho_m &= \sum_m \text{Tr}(M_m \rho M_m^\dagger) \frac{M_m \rho M_m^\dagger}{\text{Tr}(M_m \rho M_m^\dagger)} \\ &= \sum_m M_m \rho M_m^\dagger, \end{aligned} \quad (3)$$

which can be taken as a quantum evolution generated by the measurement. This process is often characterized as a *quantum channel* $\rho \mapsto \mathcal{E}(\rho) \equiv \sum_m M_m \rho M_m^\dagger$, and the set of $\{M_m\}$ is called *Kraus operators*. In this paper, the measurement operators play the role of Kraus operators.

B. Spin-1/2 particle as qubit

In the standard model of particle physics, matter particles (leptons and quarks) are all spin-1/2 fermions. Baryons including protons and neutrons that are made of quarks are also fermions. The ground states of octet baryons (n , p , Σ^\pm , Σ^0 , Λ , Ξ^- , Ξ^0) are all spin-1/2 particles. When we focus solely on the spin degree of freedom, we can map these spin-1/2 particles to the ‘‘qubits’’ which originate from QIS and refer to two-level quantum systems. Then the spin state of the particle along the spin quantization direction z can be expressed by a qubit denoted as $|0\rangle \equiv |\uparrow_z\rangle$ and $|1\rangle \equiv |\downarrow_z\rangle$. In the context of QIS, the density operator describing a qubit can be put in Bloch representation as

$$\rho = \frac{1}{2} (\mathbb{1} + \boldsymbol{\sigma} \cdot \mathbf{s}), \quad (4)$$

where $\boldsymbol{\sigma} = (\sigma_x, \sigma_y, \sigma_z)$ is the vector of three Pauli matrices, $\mathbb{1}$ denotes the 2×2 unity matrix, and the vector \mathbf{s} is called *Bloch vector* or polarization vector to describe the polarization of the qubit. The Bloch vector \mathbf{s} can be obtained by $\mathbf{s} = \langle \boldsymbol{\sigma} \rangle = \text{Tr}(\rho \boldsymbol{\sigma})$.

C. Decay width and parameters

Hyperons such as Λ , Σ , and Ξ are heavier than protons and neutrons and contain one or more strange quarks. In this work, we focus on hyperon decays. A typical hyperon decay is to another spin-1/2 baryon B' accompanied by a spin-0 meson M denoted as $B \rightarrow B' M$. According to the effective Lagrangian, the decay matrix element reads [32],

$$\mathcal{A}_{B \rightarrow B' M} = G_F m_M^2 \bar{u}_B (C_1 - C_2 \gamma_5) u_{B'}, \quad (5)$$

where G_F is the Fermi constant, m_M is the meson mass, and C_1 and C_2 are parity-violating S -wave and parity-conserving P -wave decay amplitudes. The partial decay width is given by

$$\Gamma = \frac{G_F^2 m_M^4 |\mathbf{q}|}{4\pi m_B} (m_{B'} + E_{B'}) (|S|^2 + |P|^2), \quad (6)$$

where m_B and $m_{B'}$ are the masses of the mother and daughter baryons respectively, \mathbf{q} and $E_{B'} = \sqrt{|\mathbf{q}|^2 + m_{B'}^2}$ are the momentum and the energy of the daughter baryon in the rest frame of the mother baryon respectively, and the S and P -wave amplitudes in Eq. (6) are connected with C_1 and C_2 in Eq. (5) by $S = C_1$ and $P = -|\mathbf{q}|C_2/(m_{B'} + E_{B'})$. These S and P amplitudes are Lorentz scalars and are fixed for the two-body decay. In the decay angular's distribution, we introduce three real parameters [33]

$$\alpha = \frac{2\text{Re}(S^*P)}{|S|^2 + |P|^2}, \quad \beta = \frac{2\text{Im}(S^*P)}{|S|^2 + |P|^2}, \quad \gamma = \frac{|S|^2 - |P|^2}{|S|^2 + |P|^2}, \quad (7)$$

which satisfy $\alpha^2 + \beta^2 + \gamma^2 = 1$, so α , β and γ are all in the range $[-1, 1]$. Note that one can use another parameterization $\beta = \sqrt{1 - \alpha^2} \sin \phi$ and $\gamma = \sqrt{1 - \alpha^2} \cos \phi$ with $\phi \in (-\pi, \pi]$.

III. DECAY OF SPIN-1/2 HYPERONS

In this section, we present our description of hyperon decays based on the theory of generalized quantum measurement. We mainly focus on the angular distribution of the daughter particle (baryon) and its connection with the generalized measurement description.

A. Angular distribution of daughter particle

To study the angular distribution of the outgoing baryon, we can write $\Gamma_{B \rightarrow B'M}$ derived from Eq. (5) in the form of an angular integration

$$\Gamma \propto \int \sum_{i=\pm} |\chi_{B'}^i (S + P\boldsymbol{\sigma} \cdot \mathbf{n}) \chi_B|^2 d\Omega, \quad (8)$$

where χ_B and $\chi_{B'}$ represent spinors of mother and daughter baryons respectively, and $\mathbf{n} \equiv \mathbf{q}/|\mathbf{q}|$ represents the momentum direction of B' . The summation indicates the average over daughter baryon's spin state. We can rewrite Eq. (8) in a new form as

$$\frac{1}{\Gamma} \frac{d\Gamma}{d\Omega} = \text{Tr}(M_{\mathbf{n}} \rho_B M_{\mathbf{n}}^\dagger), \quad (9)$$

where ρ_B denotes the spin density matrix for the mother baryon B , $d\Omega = d\mathbf{n} = d\cos\theta d\phi$, and the operator $M_{\mathbf{n}}$ is defined as

$$M_{\mathbf{n}} \equiv \frac{1}{\sqrt{4\pi(|S|^2 + |P|^2)}} (S + P\boldsymbol{\sigma} \cdot \mathbf{n}). \quad (10)$$

We see in Eq. (9) that the determination of the angular distribution implies a generalized measurement characterized by the measurement operator $M_{\mathbf{n}}$. In this way, the particle decay can be regarded as a kind of generalized measurement process. The only difference here is

that the discrete measurement outcome m described in Sec. II A to a continuous direction \mathbf{n} for the outgoing daughter baryon in experiments. It is necessary to validate the positive semidefiniteness and completeness of $\{M_{\mathbf{n}}\}$ as

$$M_{\mathbf{n}}^\dagger M_{\mathbf{n}} = \frac{1}{4\pi} (\mathbb{1} + \alpha\boldsymbol{\sigma} \cdot \mathbf{n}) \geq 0, \quad \text{for } |\alpha| \leq 1$$

$$\int M_{\mathbf{n}}^\dagger M_{\mathbf{n}} d\Omega = \mathbb{1}. \quad (11)$$

These two criteria ensure that $\{M_{\mathbf{n}}\}$ are legitimate measurement operators in QIS.

After defining the measurement operators, we proceed to calculate the decay process in this approach. According to the quantum measurement postulate, the probability for the momentum direction of the daughter baryon along \mathbf{n} is given by $\mathcal{P}(\mathbf{n}) = \text{Tr}(M_{\mathbf{n}} \rho_B M_{\mathbf{n}}^\dagger)$, which exactly equals to $(1/\Gamma)d\Gamma/d\Omega$ in Eq. (9). Given the initial spin density operator

$$\rho_B = \frac{1}{2}(\mathbb{1} + \boldsymbol{\sigma} \cdot \mathbf{s}_B), \quad (12)$$

as in Eq. (4), the resulting probability or the angular distribution reads

$$\mathcal{P}(\mathbf{n}) = \text{Tr}(M_{\mathbf{n}} \rho_B M_{\mathbf{n}}^\dagger) = \frac{1}{\Gamma} \frac{d\Gamma_{B \rightarrow B'M}}{d\Omega} = \frac{1}{4\pi} (1 + \alpha\mathbf{s}_B \cdot \mathbf{n}), \quad (13)$$

which was first derived in Ref. [34].

Now we look at the polarization of the daughter baryon. According to the quantum measurement postulate, the spin density operator of the daughter baryon can be obtained via the post-measurement state in Eq. (2) as

$$\rho_{B'}(\mathbf{n}) = \frac{M_{\mathbf{n}} \rho_B M_{\mathbf{n}}^\dagger}{\text{Tr}(M_{\mathbf{n}} \rho_B M_{\mathbf{n}}^\dagger)}$$

$$= \frac{1}{2} (\mathbb{1} + \boldsymbol{\sigma} \cdot \mathbf{s}_{B'}), \quad (14)$$

where $\mathbf{s}_{B'}$ is the polarization vector of the daughter baryon in the mother baryon's rest frame as a function of \mathbf{n} . By substituting ρ_B in Eq. (12) and $M_{\mathbf{n}}$ in Eq. (10) into Eq. (14), we obtain

$$\mathbf{s}_{B'} = \frac{(\alpha + \mathbf{s}_B \cdot \mathbf{n})\mathbf{n} + \beta(\mathbf{s}_B \times \mathbf{n}) + \gamma\mathbf{n} \times (\mathbf{s}_B \times \mathbf{n})}{1 + \alpha\mathbf{s}_B \cdot \mathbf{n}}, \quad (15)$$

where parameters α , β and γ are defined in Eq. (7). The explicit expression of $\mathbf{s}_{B'}$ in Eq. (15) was initially derived by Lee and Yang [33], but here we rederived it in the language of generalized quantum measurement.

We can look at the decay process as a quantum channel induced by $\{M_{\mathbf{n}}\}$. In the hyperon decay process, the daughter baryon may fly in any direction \mathbf{n} associated with the probability $\mathcal{P}(\mathbf{n})$, which is just the angular distribution of the daughter baryon in Eq. (13) that can be detected in particle physics experiments. With the daughter's spin density operator $\rho_{B'}(\mathbf{n})$, we have an

ensemble $\{\mathcal{P}(\mathbf{n}), \rho_{B'}(\mathbf{n})\}$. According to the generalized measurement postulate in Eq. (3), this post-measurement ensemble can be interpreted as a quantum evolution in the channel \mathcal{E} defined as

$$\begin{aligned} \mathcal{E}(\rho_B) &= \int d\Omega M_{\mathbf{n}} \rho_B M_{\mathbf{n}}^\dagger \equiv \int d\Omega \mathcal{E}_{\mathbf{n}}(\rho_B) \\ &= \frac{1}{2} \left(\mathbf{1} + \frac{1+2\gamma}{3} \boldsymbol{\sigma} \cdot \mathbf{s}_B \right), \end{aligned} \quad (16)$$

which is actually the ensemble average of the daughter baryon's spin density operator $\bar{\rho}_{B'} = \mathcal{E}(\rho_B)$, and the term $(1+2\gamma)\mathbf{s}_B/3$ represents the average polarization of the daughter baryon in the rest frame of the mother hyperon.

In summary, we have established in this subsection the quantum measurement interpretation for the nonleptonic decay of spin-1/2 hyperons. In the next subsection, we will introduce an alternative representation for the decay process.

B. Bloch-Fano representation

As we mentioned in subsec. II B, a single qubit can be expressed in a Bloch form as $\rho = (1/2) \sum_{\mu=0}^3 r_\mu \sigma_\mu$ with $\sigma_0 = \mathbf{1}$ and $r_\mu \equiv [1|\mathbf{r}]^T$. Here the four coefficients r_μ has been put into a 4×1 column vector. For the initial spin density operator ρ_B , we have $\mathbf{s}_{B\mu} = [1|\mathbf{s}_B]^T$ following Eq. (12). For the unnormalized density operator $\tilde{\rho}_{B'}$ resulting from the measurement $\tilde{\rho}_{B'} = M_{\mathbf{n}} \rho_B M_{\mathbf{n}}^\dagger$, it can also be expressed in the Bloch representation as $\tilde{\rho}_{B'} = (1/2) \sum_{\mu=0}^3 \tilde{r}_\mu \sigma_\mu$ with $\tilde{r}_\mu \equiv [\tilde{r}_0|\tilde{\mathbf{r}}]^T$. As a consequence, the act of $M_{\mathbf{n}}$ can be interpreted as a mapping $\mathcal{E}_{\mathbf{n}}(\rho_B)$ that transforms s_B^μ to \tilde{r}_μ .

Without the loss of generality, we assume $\mathbf{n} = \hat{\mathbf{z}} = (0, 0, 1)^T$. According to Eq. (14) and Eq. (15), the mapping $\mathcal{E}_{\mathbf{n}}$ reads

$$\begin{aligned} 1 &\mapsto \tilde{r}_0 = \frac{1}{4\pi} (1 + \alpha \hat{\mathbf{z}} \cdot \mathbf{s}_B), \\ \mathbf{s}_B &\mapsto \tilde{\mathbf{r}} = \frac{1}{4\pi} (\mathcal{O}_z \mathbf{s}_B + \alpha \hat{\mathbf{z}}), \end{aligned} \quad (17)$$

where \mathcal{O}_z is a 3×3 matrix

$$\mathcal{O}_z = \begin{bmatrix} \gamma & \beta & 0 \\ -\beta & \gamma & 0 \\ 0 & 0 & 1 \end{bmatrix}, \quad (18)$$

As a result, the measurement process $\tilde{\rho}_{B'} = M_{\mathbf{n}} \rho_B M_{\mathbf{n}}^\dagger = \mathcal{E}_z(\rho_B)$ can be expressed in the matrix form,

$$\begin{aligned} \begin{bmatrix} \tilde{r}_0 \\ \tilde{\mathbf{r}} \end{bmatrix} &= \mathcal{M}_z \begin{bmatrix} 1 \\ \mathbf{s}_B \end{bmatrix} \\ \mathcal{M}_z &\equiv \frac{1}{4\pi} \begin{bmatrix} 1 & \alpha \hat{\mathbf{z}}^T \\ \alpha \hat{\mathbf{z}} & \mathcal{O}_z \end{bmatrix} = \frac{1}{4\pi} \begin{bmatrix} 1 & 0 & 0 & \alpha \\ 0 & \gamma & \beta & 0 \\ 0 & -\beta & \gamma & 0 \\ \alpha & 0 & 0 & 1 \end{bmatrix} \begin{bmatrix} 1 \\ s_B^1 \\ s_B^2 \\ s_B^3 \end{bmatrix}. \end{aligned} \quad (19)$$

For an arbitrary direction $\mathbf{n}(\theta, \phi)$ in the quantum measurement, we can use a SO(3) rotation matrix $\mathcal{R}(\phi, \theta, 0)$ to rotate $\hat{\mathbf{z}}$ to \mathbf{n} as $\mathbf{n} = \mathcal{R}\hat{\mathbf{z}}$. Thus $M_{\mathbf{n}}$ can be put into a 4×4 matrix form

$$\mathcal{M}_{\mathbf{n}} = \frac{1}{4\pi} \begin{bmatrix} 1 & \alpha \mathbf{n}^T \\ \alpha \mathbf{n} & \mathcal{O}_{\mathbf{n}} \end{bmatrix} = \begin{bmatrix} 1 & \mathbf{0}^T \\ \mathbf{0} & \mathcal{R} \end{bmatrix} \mathcal{M}_z \begin{bmatrix} 1 & \mathbf{0}^T \\ \mathbf{0} & \mathcal{R}^{-1} \end{bmatrix}, \quad (20)$$

which is merely a similarity transformation on the 4×4 matrix \mathcal{M}_z .

We can see in Eq. (20) that all information about the generalized measurement is encoded in the 4×4 matrix $\mathcal{M}_{\mathbf{n}}$. The representation in Eq. (19) and Eq. (20) are called *Bloch-Fano representation* [35–37] in QIS, which provides an alternative representation for the quantum measurement. We should note that there is no fundamental distinction between Eq. (14) and Bloch-Fano representation in Eqs. (19, 20). Moreover, the post-measurement ensemble $\mathcal{E}(\rho_B)$ also has a Bloch-Fano representation, which can be directly obtained from Eq. (16) as

$$\mathcal{E}(\rho_B) \Leftrightarrow \mathcal{M} = \begin{bmatrix} 1 & \mathbf{0}^T \\ \mathbf{0} & \frac{1+2\gamma}{3} \mathbf{1}_3 \end{bmatrix}. \quad (21)$$

Note that the Fano matrix \mathcal{M}_z in Eq. (19) is exactly the same as *aligned decay matrices* in Ref. [15, 16], where the authors derived decay matrices through the helicity amplitude method introduced by Jacob and Wick [38]. This consistency demonstrates the validity of the quantum measurement interpretation in particle decay processes. It is possible to extract Fano matrices in various decays of spin-1/2 hyperons [16], e.g., $B \rightarrow B' \ell^- \bar{\nu}_\ell$, $B \rightarrow B' \gamma$, $B \rightarrow \ell^+ \ell^-$ and $B \rightarrow B' \pi^+ \pi^-$. We should emphasize that B and B' in this paper represent baryons, not B-mesons.

C. Decay chains

It is common for the daughter baryon to undergo subsequent decay, for example, in the decay chain $B \rightarrow B_1 M_1 \rightarrow B_2 M_2 M_1$, in which B_1 decays to $B_2 M_2$. This cascading decay process can be described by *the concatenate quantum measurement*. Then the joint angular distribution or joint probability is given by

$$\begin{aligned} \mathcal{P}(\mathbf{n}_1, \mathbf{n}_2) &= \frac{1}{\Gamma} \frac{d\Gamma}{d\Omega_1 d\Omega_2} \\ &= \text{Tr} \left[M_{\mathbf{n}_2}^{1 \rightarrow 2} M_{\mathbf{n}_1}^{B \rightarrow 1} \rho_B M_{\mathbf{n}_1}^{\dagger B \rightarrow 1} M_{\mathbf{n}_2}^{\dagger 1 \rightarrow 2} \right], \end{aligned} \quad (22)$$

which is the probability that B_1 moving in the direction \mathbf{n}_1 decays to B_3 moving in the direction \mathbf{n}_2 . Here $\{M_{\mathbf{n}_1}^{B \rightarrow 1}\}$ and $\{M_{\mathbf{n}_2}^{1 \rightarrow 2}\}$ are two sets of measurement operators characterizing two decays, $B \rightarrow B_1 M_1$ and $B_1 \rightarrow B_2 M_2$, respectively.

Likewise, the decay chain can also be presented in the Bloch-Fano representation as

$$\mathcal{E}_{n2} \circ \mathcal{E}_{n1}(\rho_B) = \mathcal{M}_{n2} \mathcal{M}_{n1} s_{B\mu}, \quad (23)$$

where \mathcal{M}_{n1} and \mathcal{M}_{n2} are Fano matrices in the form of Eq. (20). Similarly, the concatenate quantum measurement in Eq. (22) can be extended to longer decay chains.

IV. JOINT DECAY OF $B\bar{B}$ AND TWO-QUBIT CORRELATIONS

In this section, we will give a generalized quantum measurement introduced in Sec. III for the joint decay of $B\bar{B}$ to $B'\bar{B}'$ and study the correlation between $B\bar{B}$ and $B'\bar{B}'$.

If we only consider the spin degree of freedom for two spin-1/2 particles, their joint state can be written in a general form

$$\rho_{B\bar{B}} = \frac{1}{4} \left(\mathbb{1}_4 + \mathbf{s}_B \cdot \boldsymbol{\sigma} \otimes \mathbb{1}_2 + \mathbb{1}_2 \otimes \mathbf{s}_{\bar{B}} \cdot \boldsymbol{\sigma} + \sum_{i,j} C_{ij} \sigma_i \otimes \sigma_j \right), \quad (24)$$

where $i, j = 1, 2, 3$, $\mathbb{1}_n$ is the $n \times n$ unity matrix, \mathbf{s}_B and $\mathbf{s}_{\bar{B}}$ are spin polarization vectors for B and \bar{B} respectively, and C_{ij} is a 3×3 real matrix for the spin correlation between B and \bar{B} . So there are 15 real parameters in $\rho_{B\bar{B}}$ corresponding to $s_B^i = \langle \sigma_i \otimes \mathbb{1}_2 \rangle$, $s_{\bar{B}}^i = \langle \mathbb{1}_2 \otimes \sigma_i \rangle$ and $C_{ij} = \langle \sigma_i \otimes \sigma_j \rangle$. The Hilbert spaces associated with spin states of B and \bar{B} are denoted as \mathcal{H}_B and $\mathcal{H}_{\bar{B}}$ respectively, thus $\rho_{B\bar{B}}$ describes a quantum state in the joint Hilbert space $\mathcal{H}_B \otimes \mathcal{H}_{\bar{B}}$. The one particle density operator can be obtained by taking the partial trace $\rho_B = \text{Tr}_{\bar{B}}(\rho_{B\bar{B}}) = \frac{1}{2}(\mathbb{1} + \mathbf{s}_B \cdot \boldsymbol{\sigma})$ and $\rho_{\bar{B}} = \text{Tr}_B(\rho_{B\bar{B}}) = \frac{1}{2}(\mathbb{1} + \mathbf{s}_{\bar{B}} \cdot \boldsymbol{\sigma})$, which reduces to Eq. (4) for one qubit.

A. Joint decay of baryon-antibaryon with spin correlation

We consider the joint decay $B\bar{B} \rightarrow B'M\bar{B}'\bar{M}$ with spin correlation. According to the quantum measurement postulate, a joint decay process can be regarded as *parallel quantum measurement*. So the joint probability for this parallel measurement is given by

$$\mathcal{P}(\mathbf{n}, \bar{\mathbf{n}}) = \text{Tr} \left[\left(M_{\mathbf{n}} \otimes \bar{M}_{\bar{\mathbf{n}}} \right) \rho_{B\bar{B}} \left(M_{\mathbf{n}}^\dagger \otimes \bar{M}_{\bar{\mathbf{n}}}^\dagger \right) \right], \quad (25)$$

similar to Eq. (14), where \mathbf{n} or $\bar{\mathbf{n}}$ are momentum directions of B' and \bar{B}' respectively, and $\{M_{\mathbf{n}}\}$ as well as $\{\bar{M}_{\bar{\mathbf{n}}}\}$ are measurement operators acting on \mathcal{H}_B and $\mathcal{H}_{\bar{B}}$ respectively. In comparison with Eq. (13), the joint probability is actually the joint angular distribution of the daughter baryon and antibaryon. By substituting

$M_{\mathbf{n}}$ and $\bar{M}_{\bar{\mathbf{n}}}$ in the form of Eq. (10) together with $\rho_{B\bar{B}}$ from Eq. (24) into Eq. (25), the joint angular distribution is given as

$$\frac{1}{\bar{\Gamma}} \frac{d\Gamma(B\bar{B} \rightarrow B'M\bar{B}'\bar{M})}{d\Omega_{\mathbf{n}} d\Omega_{\bar{\mathbf{n}}}} = \frac{1}{(4\pi)^2} \left(1 + \alpha_B \mathbf{s}_B \cdot \mathbf{n} + \alpha_{\bar{B}} \mathbf{s}_{\bar{B}} \cdot \bar{\mathbf{n}} + \alpha_B \alpha_{\bar{B}} \sum_{i,j} C_{ij} n_i \bar{n}_j \right), \quad (26)$$

where α_B and $\alpha_{\bar{B}}$ are decay parameters defined in Eq. (7) associated with B and \bar{B} respectively.

The similar results can be found in Ref. [19, 39] in the study of the correlated $t\bar{t}$ decay. The joint angular distribution in Eq. (26) is derived in the generalized measurement approach. We note that the distribution in Eq. (25) is different from the one in Eq. (22), because the former describes the joint decay of $B\bar{B}$, while the latter describes the decay chain of B .

B. Charmonium decays and quantum entanglement

The charmonium ($c\bar{c}$) decays to hyperon-antihyperon provide an ideal place to test the quantum entanglement and correlation in the joint decay of hyperon-antihyperon. From Eqs. (24) and (26) we see that $\rho_{B\bar{B}}$ can be probed or extracted by the joint angular distribution in the decay of hyperon-antihyperon in experiments.

In this work, we focus on the decays of spin-0 charmonia $\eta_c/\chi_{c0} \rightarrow \Lambda\bar{\Lambda} \rightarrow p\pi^-\bar{p}\pi^+$ which were discussed in Ref. [13, 40]. Since η_c is a pseudoscalar particle, the spin state of $\Lambda\bar{\Lambda}$ should be spin singlet corresponding to the following density operator

$$\rho_{\Lambda\bar{\Lambda}}(\eta_c) = |\Psi^-\rangle \langle \Psi^-| = \frac{1}{4} \left(\mathbb{1}_4 - \sum_i \sigma_i \otimes \sigma_i \right), \quad (27)$$

where $|\Psi^-\rangle$ denotes spin singlet $|\Psi^-\rangle = (|01\rangle - |10\rangle)/\sqrt{2}$. From Eq. (27), there is no polarization for Λ and $\bar{\Lambda}$ since $\mathbf{s}_\Lambda = \mathbf{s}_{\bar{\Lambda}} = \mathbf{0}$, and the spin correlation matrix reads $C = \text{diag}\{-1, -1, -1\}$. The spin state of $\Lambda\bar{\Lambda}$ in the decay of the scalar particle χ_{c0} is the spin-0 state of the spin triplet in the spin quantization direction, so the spin density operator for $\Lambda\bar{\Lambda}$ reads

$$\rho_{\Lambda\bar{\Lambda}}(\chi_{c0}) = |\Psi^+\rangle \langle \Psi^+| = \frac{1}{4} \left(\mathbb{1}_4 + \sum_{i,j} C_{ij} \sigma_i \otimes \sigma_j \right), \quad (28)$$

where $|\Psi^+\rangle = (|01\rangle + |10\rangle)/\sqrt{2}$ is the Bell state in the spin triplet. We see that there is no polarization for Λ and $\bar{\Lambda}$ and the spin correlation matrix is $C = \text{diag}\{+1, +1, -1\}$. Using Eqs. (27) and (28) in Eq. (26),

we obtain the joint angular distributions as

$$\begin{aligned} \frac{1}{\Gamma} \frac{d\Gamma_{\eta_c}}{d\Omega_{\mathbf{n}}d\Omega_{\bar{\mathbf{n}}}} &= \frac{1}{(4\pi)^2} (1 - \alpha_{\Lambda}\alpha_{\bar{\Lambda}}\mathbf{n} \cdot \bar{\mathbf{n}}), \\ \frac{1}{\Gamma} \frac{d\Gamma_{\chi_{c0}}}{d\Omega_{\mathbf{n}}d\Omega_{\bar{\mathbf{n}}}} &= \frac{1}{(4\pi)^2} [1 + \alpha_{\Lambda}\alpha_{\bar{\Lambda}}(n_x\bar{n}_x + n_y\bar{n}_y - n_z\bar{n}_z)], \end{aligned} \quad (29)$$

where \mathbf{n} and $\bar{\mathbf{n}}$ are momentum directions for p and \bar{p} respectively.

From the above cases, it is evident that the spin density operator $\rho_{\Lambda\bar{\Lambda}}$ can be reconstructed tomographically from the joint distribution of $p\bar{p}$ in the subsequent decay $\Lambda\bar{\Lambda} \rightarrow p\pi^-\bar{p}\pi^+$. The reconstruction of $\rho_{\Lambda\bar{\Lambda}}$ enables a comprehensive analysis of quantum correlation in $\Lambda\bar{\Lambda}$ system.

Generally speaking, the quantum correlation or entanglement in $\rho_{B\bar{B}}$ is fully encoded in C_{ij} . There are various types of quantum correlation [19]. In this work, we only consider Bell nonlocality in testing the violation of the CHSH inequality. The maximum value of the Bell operator associated with the CHSH inequality can be directly calculated through C_{ij} in $\rho_{B\bar{B}}$. According to Ref. [41], the maximum value of the Bell operator reads $\langle \mathcal{B}_{\text{CHSH}} \rangle_{\text{max}} = 2\sqrt{\lambda_1 + \lambda_2}$, where λ_1 and λ_2 are two largest eigenvalues of the matrix $C^T C$. Thus, from Eqs. (27) and (28) in decays of η_c and χ_{c0} , the upper bound $2\sqrt{2}$ in the CHSH inequality has been approached in $\Lambda\bar{\Lambda}$. This violation lies in the fact that the spin states of $\Lambda\bar{\Lambda}$ are the Bell states $|\Psi^{\pm}\rangle$ that are maximally entangled.

V. QUANTUM SIMULATION

In this section, we will perform quantum simulation for the decay of hyperon-antihyperon and present the test of the CHSH inequality through the spin correlation in the hyperon-antihyperon system.

A. Simulation for generalized measurement process

Similar to $M_{\mathbf{n}}$ for the hyperon decay in Eq. (10), $\bar{M}_{\mathbf{n}}$ for the antihyperon decay is defined as

$$\bar{M}_{\mathbf{n}} = \frac{1}{\sqrt{4\pi}} \frac{1}{\sqrt{|\bar{S}|^2 + |\bar{P}|^2}} (\bar{S} + \bar{P}\boldsymbol{\sigma} \cdot \mathbf{n}), \quad (30)$$

which can be obtained from Eq. (10) by simply making the replacement $S \rightarrow \bar{S}$ and $P \rightarrow \bar{P}$.

In order to perform the simulation on the digital quantum computer, the measurement operators $\{M_{\mathbf{n}}\}$ must be embedded into unitary operators. It can be verified

that the block matrix

$$U_{\mathbf{n}} \equiv \frac{1}{\sqrt{2(|S|^2 + |P|^2)}} \begin{bmatrix} S + P\boldsymbol{\sigma} \cdot \mathbf{n} & P^* - S^*\boldsymbol{\sigma} \cdot \mathbf{n} \\ S - P\boldsymbol{\sigma} \cdot \mathbf{n} & P^* + S^*\boldsymbol{\sigma} \cdot \mathbf{n} \end{bmatrix}, \quad (31)$$

is unitary, and $M_{\mathbf{n}}$ is embedded as the upper-left block. From the definition of $M_{\mathbf{n}}$ in Eq. (10), it can be expressed by $M_{\mathbf{n}} = U(\mathcal{R})M_{\hat{\mathbf{z}}}U(\mathcal{R})^\dagger$, where $U(\mathcal{R})$ denotes a SU(2) rotation isomorphic to $\mathcal{R}(\phi, \theta, 0)$. As a consequence, the unitary operator $U_{\mathbf{n}}$ can be obtained by performing a similarity transformation on $U_{\hat{\mathbf{z}}}$, as $U_{\mathbf{n}} = [\mathbb{1} \otimes U(\mathcal{R})]U_{\hat{\mathbf{z}}}[\mathbb{1} \otimes U(\mathcal{R})^\dagger]$. Similarly the unitary operator $\bar{U}_{\mathbf{n}}$ for the antihyperon decay can also be defined by the replacement $S \rightarrow \bar{S}$ and $P \rightarrow \bar{P}$.

Following this, the quantum circuit for simulating the joint decay of $\Lambda\bar{\Lambda} \rightarrow p\pi^-\bar{p}\pi^+$ is presented in Fig. 1, where the spin states of $\Lambda\bar{\Lambda}$ are prepared to be in the Bell states $|\Psi^{\pm}\rangle$ resulted from η_c/χ_{c0} decay as discussed in Sec. IV. Figure 1 indicates that the measurement operators have been successfully embedded into unitary operators, and the quantum information contained in $\Lambda\bar{\Lambda}$ can be extracted from ancilla qubits.

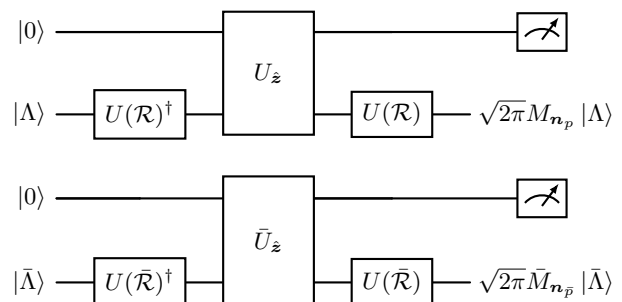


Figure 1. The quantum circuit for generalized measurements. The spin states of Λ and $\bar{\Lambda}$ are prepared to be in the Bell states $|\Psi^{\pm}\rangle$. The additional two ancilla qubits are initialized to be in $|0\rangle$. $U_{\hat{\mathbf{z}}}$ and $\bar{U}_{\hat{\mathbf{z}}}$ are the unitary gates in which the measurement operators $M_{\hat{\mathbf{z}}}$ and $\bar{M}_{\hat{\mathbf{z}}}$ are embedded. $U(\mathcal{R})$ and $U(\bar{\mathcal{R}})$ are SU(2) rotation gates. The measurements are performed on two ancilla qubits by which the quantum information in $\Lambda\bar{\Lambda}$ can be extracted.

The simulation has been performed on simulators and the superconducting quantum computer *Quafu* developed in Beijing Academy of Quantum Information Sciences. The simulation results are shown in Fig. 2, which agree with the theoretical expectation that they enter the quantum region $[-2\sqrt{2}, -2) \cup (2, 2\sqrt{2}]$ and reach the maximum $2\sqrt{2}$. Thus we conclude that there is maximum violation of the CHSH inequality in $\Lambda\bar{\Lambda}$ from charmium decays, which coincides with the result in Sec. IV. However, the violation of the CHSH inequality on real quantum computers turns out to be very weak. This is due to the noise in the real platform, which decreases the quantumness between two qubits. The details of our

quantum simulation are shown in Appendix. A.

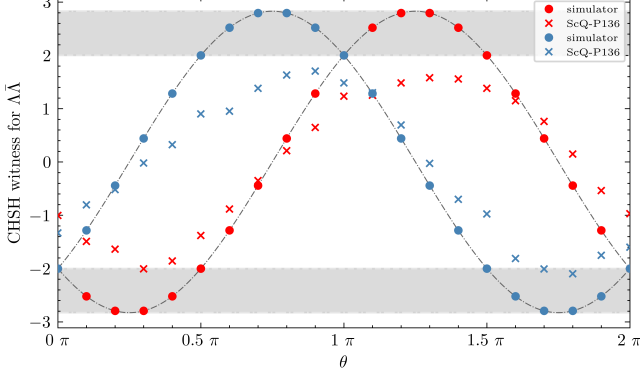


Figure 2. The CHSH witness in the simulation of the entangled states of $\Lambda\bar{\Lambda}$. Solid circles are results on noiseless simulator while cross symbols are results on the superconducting quantum computer with 136 qubits. The red/blue symbols represent the initial entangled states $|\Psi^-\rangle/|\Psi^+\rangle$ for $\Lambda\bar{\Lambda}$. The shadow area is the quantum region $[-2\sqrt{2}, -2) \cup (+2 + 2\sqrt{2}]$.

B. Simulation for depolarizing channel

As we discussed in Eq. (16), the average spin density matrix of the daughter baryon in $B \rightarrow B'M$ is $\bar{\rho}_{B'} = \mathcal{E}(\rho_B)$. In the viewpoint of QIS, the post-measurement ensemble can be interpreted as a quantum evolution characterized by the quantum channel. We notice that Eq. (16) can be regarded as a single-qubit depolarizing channel as

$$\rho_B \mapsto \rho_{B'} \equiv \mathcal{E}(\rho_B) = \mathcal{P} \frac{\mathbb{1}}{2} + (1 - \mathcal{P})\rho_B, \quad (32)$$

where $\mathcal{P} \equiv (2 - 2\gamma_B)/3$. We have a similar form for antibaryon: $\rho_{\bar{B}'} \equiv \mathcal{E}(\rho_{\bar{B}})$ with $\bar{\mathcal{P}} \equiv (2 - 2\gamma_{\bar{B}})/3$. Then the average spin density matrix for $B'\bar{B}'$ from the joint decay of $B\bar{B} \rightarrow B'M\bar{B}'\bar{M}$ can be presented as

$$\begin{aligned} \rho_{B'\bar{B}'} &= \mathcal{E} \otimes \bar{\mathcal{E}}(\rho_{B\bar{B}}) \\ &= \frac{1}{4} \left[\mathbb{1} + (1 - \mathcal{P})\boldsymbol{\sigma} \cdot \mathbf{s}_B \otimes \mathbb{1} + (1 - \bar{\mathcal{P}})\mathbb{1} \otimes \boldsymbol{\sigma} \cdot \mathbf{s}_{\bar{B}} \right. \\ &\quad \left. + (1 - \mathcal{P})(1 - \bar{\mathcal{P}}) \sum_{i,j} C_{ij} \sigma_i \otimes \sigma_j \right]. \end{aligned} \quad (33)$$

Since the decay processes of B and \bar{B} are not correlated, the two-qubit channel can be described as a tensor product of two independent single-qubit depolarizing channels $\mathcal{E} \otimes \bar{\mathcal{E}}$. From Eq. (33), the polarization vectors decrease by factors $(1 - \mathcal{P})$ and $(1 - \bar{\mathcal{P}})$, while the spin correlation decreases by a factor $(1 - \mathcal{P})(1 - \bar{\mathcal{P}})$. This means that the spin correlation is suppressed in decay processes. The suppression of the spin correlation may lead to the satisfaction of the CHSH inequality, since the maximal

violation also decreases by the factor $(1 - \mathcal{P})(1 - \bar{\mathcal{P}})$, which has been discussed in Ref. [12].

We now perform a simulation based on decays $\eta_c/\chi_{c0} \rightarrow \Lambda\bar{\Lambda} \rightarrow p\pi^-\bar{p}\pi^+$. The simulation results for the channel $\rho_{p\bar{p}} = \mathcal{E} \otimes \bar{\mathcal{E}}(\rho_{\Lambda\bar{\Lambda}})$ are presented in Fig. 3. In principle, the maximum value of the Bell operator in $p\bar{p}$ becomes

$$\langle \mathcal{B}_{\text{CHSH}} \rangle_{\text{max}} = \left(\frac{1 + 2\gamma_{\Lambda}}{3} \right)^2 2\sqrt{2}, \quad (34)$$

with $\gamma_{\Lambda} = \gamma_{\bar{\Lambda}}$. The data for Λ hyperon gives $\gamma_{\Lambda} \approx 0.66$ in PDG [32]. Thus, the maximum value is $\langle \mathcal{B}_{\text{CHSH}} \rangle_{\text{max}} \approx 1.69 < 2$, which means the spin correlation of $p\bar{p}$ cannot not reach the quantum bound and does not show the property of nonlocality.

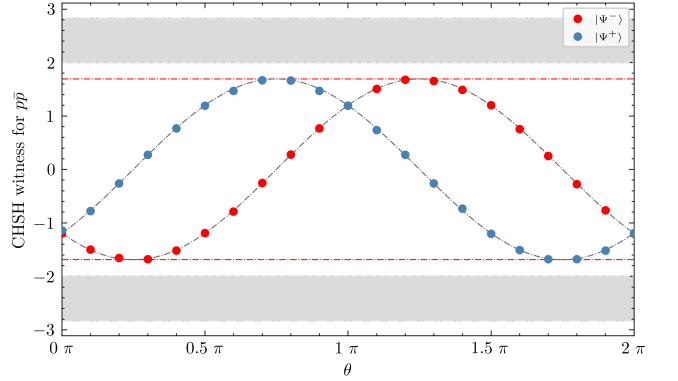


Figure 3. The simulation results for $p\bar{p}$ in the decay $\eta_c/\chi_{c0} \rightarrow \Lambda\bar{\Lambda} \rightarrow p\pi^-\bar{p}\pi^+$ and test of the CHSH inequality. The solid circles denote the results on the noiseless simulator. The red/blue symbols represent $p\bar{p}$ produced in the subsequent decay of $\Lambda\bar{\Lambda}$ in prepared initial states $|\Psi^-\rangle/|\Psi^+\rangle$. The shadow area is the quantum region of $[-2\sqrt{2}, -2) \cup (+2 + 2\sqrt{2}]$, and the red dashdotted lines indicate the bound in Eq. (34).

In Fig. 3, we can observe that the simulation results are in agreement with our theoretical expectation that the spin correlation in decay daughters decreases in decay processes.

VI. PROJECTIVE MEASUREMENT AND UNITARY EVOLUTION

In this section, we will discuss the origin of generalized measurement and its connection with particle decay/scattering processes.

In the hyperon decay $B \rightarrow B'M$, since M is a pseudoscalar meson, we can neglect its quantum state. The quantum state of the mother hyperon is $|B\rangle = |\text{momentum}\rangle \otimes |\text{spin}\rangle$ in the Hilbert space $\mathcal{H}_{\text{momentum}} \otimes \mathcal{H}_{\text{spin}}$. The general decay process can be described by a unitary evolution U called the scattering matrix S in quantum field theory. In the decay, the outgoing daughter baryon is detected in the direction $\mathbf{n}(\theta, \phi)$ with the angular distribution in experiments.

From the perspective of QIS, the decay process can be described as a unitary evolution governed by the Hamiltonian (or Lagrangian) of the system, $U(\rho_{\text{momentum}} \otimes \rho_{\text{spin}})U^\dagger$. Then the decay takes place by an emission of daughter particles in a certain direction, which indicates that a projective measurement is performed on the evolved system as $\Pi_{\theta\phi}U(\rho_{\text{momentum}} \otimes \rho_{\text{spin}})U^\dagger\Pi_{\theta\phi}^\dagger$, where the measurement operators are defined as projectors $\Pi_{\theta\phi} = |\theta\phi\rangle\langle\theta\phi| \in \mathcal{H}_{\text{momentum}}$. Here the quantum state of the daughter baryon $\rho_{B'} = U(\rho_{\text{momentum}} \otimes \rho_{\text{spin}})U^\dagger$ has been projected into the direction $\mathbf{n}(\theta, \phi)$ in momentum space. Note that the momentum magnitude $|\mathbf{p}|$ is fixed by the energy-momentum conservation in the two-body decay.

According to the quantum measurement postulate discussed in Sec. II A, the probability for finding the daughter baryon in the \mathbf{n} direction reads

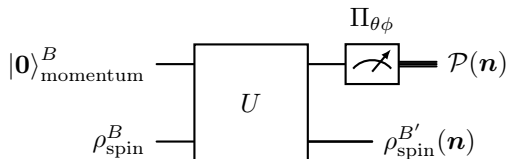
$$\mathcal{P}(\mathbf{n}) \propto \text{Tr} \left(\Pi_{\theta\phi} U (\rho_{\text{momentum}} \otimes \rho_{\text{spin}}) U^\dagger \Pi_{\theta\phi}^\dagger \right), \quad (35)$$

where $\mathcal{P}(\mathbf{n})$ is just the angular distribution $(1/\Gamma)(d\Gamma/d\Omega)$. In decay or scattering processes, the momenta of initial particles are pre-determined. In the decay process, the initial momentum state is denoted as $|\mathbf{0}\rangle = |\mathbf{p} = \mathbf{0}\rangle$ by choosing the rest frame of mother particle, hence we have $\rho_{\text{momentum}}^B = |\mathbf{0}\rangle\langle\mathbf{0}|$ in Eq. (35). Since the initial momentum state is fixed, and the density matrix only contains the spin degree of freedom for the daughter baryon and can be obtained by taking the partial trace over momentum

$$\rho_{\text{spin}}^{B'}(\mathbf{n}) \propto \text{Tr}_{\text{momentum}} \left(\Pi_{\theta\phi} U |\mathbf{0}\rangle \rho_{\text{spin}}^B \langle\mathbf{0}| U^\dagger \Pi_{\theta\phi}^\dagger \right), \quad (36)$$

where the action $\text{Tr}_{\text{momentum}}$ discards the momentum degree of freedom. Considering Eqs. (2) and (14), it can be shown that $\rho_{\text{spin}}^{B'}(\mathbf{n}) \propto M_{\mathbf{n}} \rho_{\text{spin}}^B M_{\mathbf{n}}^\dagger$, where $\{M_{\mathbf{n}}\}$ denotes the generalized measurement operators induced by the partial trace over momentum.

A heuristic quantum circuit in demonstrating the decay $B \rightarrow B'M$ is shown as



This quantum circuit gives a pedagogical illustration of the projective measurement and unitary evolution in particle decay and scattering processes in accordance with Eqs. (35, 36). The upper wire denotes the momentum state of the mother baryon $|\mathbf{p}\rangle$, which is initialized as $|\mathbf{0}\rangle$ in the rest frame, while the lower one denotes the spin state. The unitary gate “ U ” represents the unitary S-matrix in scattering theory. After the unitary evolution, a projective measurement $\Pi_{\theta\phi}$ is performed on the momentum state, resulting in the angular distribution of the daughter baryon. Consequently, the spin density

operator $\rho_{\text{spin}}^{B'}(\mathbf{n})$ in Eq. (36) is then obtained after the projective measurement.

In quantum information theory, a unitary evolution combined with projective measurements are suffice to induce a set of generalized measurements $\{M_{\mathbf{n}}\}$ which contain both the dynamical and measurement information of the system. The generalized measurement formalism is very useful to describe decay and scattering processes in particle physics. For more details of the topic, we refer the readers to Chapter 2.2.8 of Ref. [31].

VII. SUMMARY

The particle decay processes is described as the generalized quantum measurement in quantum information theory. We consider a spin-1/2 hyperon decaying to one spin-1/2 baryon and one spin-0 meson. In this perspective, we successfully establish a correspondence between the angular distribution of the daughter baryon and the generalized measurement operator. The Bloch-Fano representation is employed to describe the quantum measurement process, which shows a direct parallelism with the decay matrices outlined in Ref. [16]. We apply this method to the joint decay of $\eta_c/\chi_{c0} \rightarrow \Lambda\bar{\Lambda} \rightarrow p\pi^+\bar{p}\pi^-$ and investigate the spin correlation in $\Lambda\bar{\Lambda}$ as well as in $p\bar{p}$ systems. The quantum simulation to test the CHSH inequality on both the simulator and real quantum computer has been done. A discussion on the connection between the particle decay and the generalized quantum measurement has been given.

The generalized measurement description can be applied to a wide range of decay and scattering processes. In particular, it offers us a QIS-based tool to analyze unknown particle decays in search for new physics, such as dark matter particles. It also opens a window for testing quantum nonlocality or other quantum properties in particle decays on quantum computers. Our results can be verified in particle experiments such as BESIII [9].

ACKNOWLEDGMENTS

We would like to thank S. Lin, D. E. Liu and R. Venugopalan for helpful discussions. And we thank H.-Z. Xu for *Quafu* software and hardware supports. This work is supported by the National Natural Science Foundation of China (NSFC) under Grant Nos. 12135011, 12305010, and by the Strategic Priority Research Program of the Chinese Academy of Sciences (CAS) under Grant No. XDB34030102.

Appendix A: Details for quantum simulation

Through the unitary embedding introduced in Sec. V, we have the unitary operators $U_{\mathbf{n}}$ and $\bar{U}_{\mathbf{n}}$ acting on the

corresponding states as

$$\begin{aligned}
U_{\mathbf{n}} : |0\rangle \otimes |\Lambda\rangle &\mapsto \underbrace{\sqrt{2\pi} |0\rangle \otimes M_{\mathbf{n}} |\Lambda\rangle}_{\Lambda \rightarrow p} \\
&+ \frac{1}{\sqrt{2(|S|^2 + |P|^2)}} |1\rangle \otimes (S - P\boldsymbol{\sigma} \cdot \mathbf{n}) |\Lambda\rangle, \\
\bar{U}_{\mathbf{n}} : |0\rangle \otimes |\bar{\Lambda}\rangle &\mapsto \underbrace{\sqrt{2\pi} |0\rangle \otimes \bar{M}_{\mathbf{n}} |\bar{\Lambda}\rangle}_{\bar{\Lambda} \rightarrow \bar{p}} \\
&+ \frac{1}{\sqrt{2(|\bar{S}|^2 + |\bar{P}|^2)}} |1\rangle \otimes (\bar{S} - \bar{P}\boldsymbol{\sigma} \cdot \mathbf{n}) |\bar{\Lambda}\rangle,
\end{aligned} \tag{A1}$$

where $|0\rangle = (1, 0)^T$, $|1\rangle = (0, 1)^T$, $|0\rangle \otimes |\Lambda\rangle = (\lambda_1, \lambda_2, 0, 0)^T$ and $|1\rangle \otimes |\Lambda\rangle = (0, 0, \lambda_1, \lambda_2)^T$ with $|\Lambda\rangle = (\lambda_1, \lambda_2)^T$, $M_{\mathbf{n}}$ is given in Eq. (10), and $\bar{M}_{\mathbf{n}}$ is given in Eq. (30) which are the measurement operators associated with the decay of Λ and $\bar{\Lambda}$ respectively. From Eq. (A1), performing the projective measurements on the ancilla registers results in

$$\begin{aligned}
\mathcal{P}(|0\rangle) &= (2\pi) \langle \Lambda | M_{\mathbf{n}}^\dagger M_{\mathbf{n}} | \Lambda \rangle = \frac{1}{2} \langle \Lambda | (1 + \alpha \boldsymbol{\sigma} \cdot \mathbf{n}) | \Lambda \rangle, \\
\mathcal{P}(|1\rangle) &= \frac{\langle \Lambda | (S^* - P^* \boldsymbol{\sigma} \cdot \mathbf{n}) (S - P \boldsymbol{\sigma} \cdot \mathbf{n}) | \Lambda \rangle}{2(|S|^2 + |P|^2)} \\
&= \frac{1}{2} \langle \Lambda | (1 - \alpha \boldsymbol{\sigma} \cdot \mathbf{n}) | \Lambda \rangle,
\end{aligned} \tag{A2}$$

which leads to the expectation value of σ_z on the ancilla qubit as

$$\langle \sigma_z \rangle_{\text{anc}} = \mathcal{P}(|0\rangle) - \mathcal{P}(|1\rangle) = \alpha \langle \Lambda | \boldsymbol{\sigma} \cdot \mathbf{n} | \Lambda \rangle = \alpha \langle \boldsymbol{\sigma} \cdot \mathbf{n} \rangle_{\Lambda}. \tag{A3}$$

We see in the above formula that the expectation value associated on the Λ qubit can be obtained from the expectation value of σ_z on the ancilla qubit $\langle \boldsymbol{\sigma} \cdot \mathbf{n} \rangle_{\Lambda} = (1/\alpha) \langle \sigma_z \rangle_{\text{anc}}$. The same result holds for $\bar{\Lambda}$. Thus, the joint expectation value of $\Lambda \bar{\Lambda}$ reads

$$\langle \boldsymbol{\sigma} \cdot \mathbf{n}_p \otimes \boldsymbol{\sigma} \cdot \mathbf{n}_{\bar{p}} \rangle_{\Lambda \bar{\Lambda}} \equiv \frac{1}{\alpha \bar{\alpha}} \langle \sigma_z \otimes \sigma_z \rangle_{\text{anc}}, \tag{A4}$$

which can be directly implemented on the quantum circuit and is adopted in our test of the CHSH inequality on the quantum computer. In our simulations, the \mathcal{CP} violation is ignored and the parameters are specified as $\alpha_{\Lambda} = -\alpha_{\bar{\Lambda}} = 0.75$ and $\phi_{\Lambda} = \phi_{\bar{\Lambda}} = 0$.

The Bell operator defined in Ref. [41] reads

$$\begin{aligned}
\langle \mathcal{B}_{\text{CHSH}} \rangle &= \langle \boldsymbol{\sigma} \cdot \hat{\mathbf{a}}_1 \otimes \boldsymbol{\sigma} \cdot \hat{\mathbf{b}}_1 \rangle + \langle \boldsymbol{\sigma} \cdot \hat{\mathbf{a}}_2 \otimes \boldsymbol{\sigma} \cdot \hat{\mathbf{b}}_1 \rangle \\
&+ \langle \boldsymbol{\sigma} \cdot \hat{\mathbf{a}}_1 \otimes \boldsymbol{\sigma} \cdot \hat{\mathbf{b}}_2 \rangle - \langle \boldsymbol{\sigma} \cdot \hat{\mathbf{a}}_2 \otimes \boldsymbol{\sigma} \cdot \hat{\mathbf{b}}_2 \rangle,
\end{aligned} \tag{A5}$$

where $\hat{\mathbf{a}}_1$, $\hat{\mathbf{a}}_2$, $\hat{\mathbf{b}}_1$ and $\hat{\mathbf{b}}_2$ are unit vectors and can be put in the zx plane. In our paper, the quantum states used

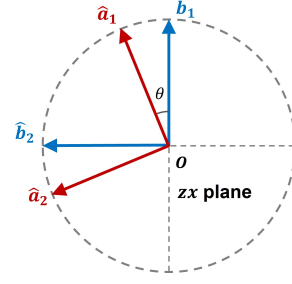


Figure 4. Orientations of four unit vectors $\hat{\mathbf{a}}_1$, $\hat{\mathbf{a}}_2$, $\hat{\mathbf{b}}_1$ and $\hat{\mathbf{b}}_2$ in zx plane.

in the test of the CHSH inequality are two Bell states $|\Psi^\pm\rangle$. For convenience, the Bell operator in Eq. (A5) is modified as

$$\begin{aligned}
\langle \mathcal{B}_{\text{CHSH}} \rangle_{\Psi^-} &= \langle \hat{\mathbf{a}}_1, \hat{\mathbf{b}}_1 \rangle + \langle \hat{\mathbf{a}}_1, \hat{\mathbf{b}}_2 \rangle - \langle \hat{\mathbf{a}}_2, \hat{\mathbf{b}}_1 \rangle + \langle \hat{\mathbf{a}}_2, \hat{\mathbf{b}}_2 \rangle, \\
\langle \mathcal{B}_{\text{CHSH}} \rangle_{\Psi^+} &= \langle \hat{\mathbf{a}}_1, \hat{\mathbf{b}}_1 \rangle + \langle \hat{\mathbf{a}}_1, \hat{\mathbf{b}}_2 \rangle + \langle \hat{\mathbf{a}}_2, \hat{\mathbf{b}}_1 \rangle - \langle \hat{\mathbf{a}}_2, \hat{\mathbf{b}}_2 \rangle,
\end{aligned} \tag{A6}$$

where $\langle \hat{\mathbf{a}}, \hat{\mathbf{b}} \rangle \equiv \langle \boldsymbol{\sigma} \cdot \hat{\mathbf{a}} \otimes \boldsymbol{\sigma} \cdot \hat{\mathbf{b}} \rangle$. For further simplification, we set the angle between $\hat{\mathbf{a}}_1$ and $\hat{\mathbf{a}}_2$ is equal to $\pi/2$, so is the angle between $\hat{\mathbf{b}}_1$ and $\hat{\mathbf{b}}_2$. Without losing generality, we assume $\hat{\mathbf{b}}_1 = \hat{\mathbf{z}}$, $\hat{\mathbf{b}}_2 = \hat{\mathbf{x}}$, $\hat{\mathbf{a}}_1 = \cos \theta \hat{\mathbf{z}} + \sin \theta \hat{\mathbf{x}}$, and $\hat{\mathbf{a}}_2 = -\sin \theta \hat{\mathbf{z}} + \cos \theta \hat{\mathbf{x}}$, see Fig. 4. The expectation values are calculated using the property $\langle \hat{\mathbf{a}}, \hat{\mathbf{b}} \rangle = \langle \hat{\mathbf{a}}, C \hat{\mathbf{b}} \rangle = \hat{\mathbf{a}}^T C \hat{\mathbf{b}}$ with C being the correlation matrix in Eq. (24). For $|\Psi^- \rangle$ we have $C = \text{diag}\{-1, -1, -1\}$, while for $|\Psi^+ \rangle$ we have $C = \text{diag}\{+1, +1, -1\}$. Finally we obtain the results for $\langle \mathcal{B}_{\text{CHSH}} \rangle$ as

$$\begin{aligned}
\langle \mathcal{B}_{\text{CHSH}} \rangle_{\Psi^-} &= -2\sqrt{2} \sin(\theta + \frac{\pi}{4}), \\
\langle \mathcal{B}_{\text{CHSH}} \rangle_{\Psi^+} &= 2\sqrt{2} \sin(\theta - \frac{\pi}{4}).
\end{aligned} \tag{A7}$$

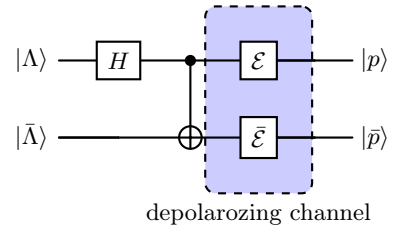


Figure 5. The quantum circuit simulating $\Lambda \bar{\Lambda} \rightarrow p \bar{p}$, where $\mathcal{E} \otimes \bar{\mathcal{E}}$ represents two depolarizing channels.

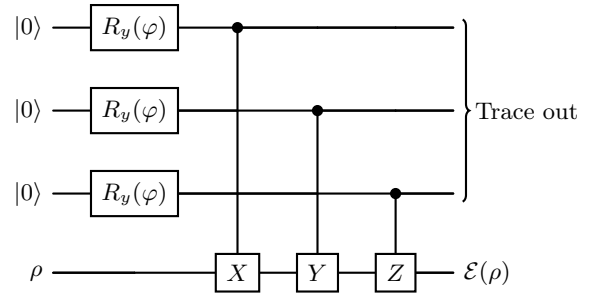


Figure 6. Circuit implementation of depolarizing channel. The first three qubits are introduced as ancillae, while the last is the system qubit representing the spin of Λ hyperon. X , Y , and Z are three Pauli gates and φ in R_y rotation gates are $\varphi = \frac{1}{2} \arccos(1 - 2\mathcal{P})$, with \mathcal{P} in Eq. (A8).

In the simulation of the spin correlation in $p\bar{p}$ in the jointed decay of $\Lambda\bar{\Lambda} \rightarrow p\pi^-\bar{p}\pi^+$, we implement the depolarizing channel by the quantum circuit in Fig. (5). The single-qubit depolarizing channel can be expressed as

$$\mathcal{E}(\rho) = \left(1 - \frac{3\mathcal{P}}{4}\right)\rho + \frac{\mathcal{P}}{4}(X\rho X + Y\rho Y + Z\rho Z), \quad (\text{A8})$$

and the details for the quantum circuit implementation are shown in Fig. (6).

-
- [1] Y. Afik and J. R. M. de Nova, *Quantum* **6**, 820 (2022).
[2] C. Altomonte and A. J. Barr, *Phys. Lett. B* **847**, 138303 (2023).
[3] J. S. Bell, *Physics Physique Fizika* **1**, 195 (1964).
[4] J. F. Clauser and M. A. Horne, *Phys. Rev. D* **10**, 526 (1974).
[5] A. Aspect, P. Grangier, and G. Roger, *Phys. Rev. Lett.* **47**, 460 (1981).
[6] J. Yin, Y. Cao, Y.-H. Li, S.-K. Liao, L. Zhang, J.-G. Ren, W.-Q. Cai, W.-Y. Liu, B. Li, H. Dai, *et al.*, *Science* **356**, 1140 (2017).
[7] The BIG Bell Test Collaboration, *Nature* **557**, 212 (2018).
[8] A. Aspect, *Quantum Unspeakeables: From Bell to Quantum Information*, edited by R. A. Bertlmann and A. Zeilinger (Springer Berlin Heidelberg, Berlin, Heidelberg, 2002) pp. 119–153.
[9] M. Ablikim *et al.* (BESIII Collaboration), *Nature Physics* **15**, 631 (2019).
[10] N. A. Törnqvist, *Found. Phys.* **11**, 171 (1981).
[11] A. S. Khan, J.-L. Li, and C.-F. Qiao, *Phys. Rev. D* **101**, 096016 (2020).
[12] C. Qian, J.-L. Li, A. S. Khan, and C.-F. Qiao, *Phys. Rev. D* **101**, 116004 (2020).
[13] S. Chen, Y. Nakaguchi, and S. Komamiya, *Prog. Theor. Exp. Phys.* **2013**, 063A01 (2013).
[14] Y. Shi and J.-C. Yang, *Eur. Phys. J. C* **80**, 116 (2020).
[15] E. Perotti, G. Fäldt, A. Kupsc, S. Leupold, and J. J. Song, *Phys. Rev. D* **99**, 056008 (2019).
[16] V. Batozskaya, A. Kupsc, N. Salone, and J. Wiechnik, *Phys. Rev. D* **108**, 016011 (2023).
[17] W. Gong, G. Parida, Z. Tu, and R. Venugopalan, *Phys. Rev. D* **106**, L031501 (2022).
[18] R. Aoude, E. Madge, F. Maltoni, and L. Mantani, *Phys. Rev. D* **106**, 055007 (2022).
[19] Y. Afik and J. R. M. de Nova, *Phys. Rev. Lett.* **130**, 221801 (2023).
[20] M. Fabbrichesi, R. Floreanini, and G. Panizzo, *Phys. Rev. Lett.* **127**, 161801 (2021).
[21] Y. Afik and J. R. M. de Nova, *Eur. Phys. J. P* **136**, 907 (2021).
[22] M. Fabbrichesi, R. Floreanini, and E. Gabrielli, *The European Physical Journal C* **83** (2023).
[23] A. J. Barr, *Physics Letters B* **825**, 136866 (2022).
[24] A. J. Barr, P. Caban, and J. Rembieliński, *Quantum* **7**, 1070 (2023).
[25] M. Fabbrichesi, R. Floreanini, E. Gabrielli, and L. Marzola, *The European Physical Journal C* **83** (2023).
[26] R. Ashby-Pickering, A. J. Barr, and A. Wierzychucka, *J. High Ener. Phys.* **2023**, 20 (2023).
[27] J. Barata, W. Gong, and R. Venugopalan, Realtime dynamics of hyperon spin correlations from string fragmentation in a deformed four-flavor schwinger model (2023), arXiv:2308.13596 [hep-ph].
[28] L.-G. Pang, H. Petersen, Q. Wang, and X.-N. Wang, *Phys. Rev. Lett.* **117**, 192301 (2016).
[29] J.-P. Lv, Z.-H. Yu, Z.-T. Liang, Q. Wang, and X.-N. Wang, Global quark spin correlations in relativistic heavy ion collisions (2024), arXiv:2402.13721 [hep-ph].
[30] X.-Q. Hao, H.-W. Ke, Y.-B. Ding, P.-N. Shen, and X.-Q. Li, *Chin. Phys. C* **34**, 311 (2010).
[31] M. A. Nielsen and I. L. Chuang, *Quantum Computation*

- and Quantum Information* (Cambridge University Press, Cambridge, 2015).
- [32] Particle Data Group, *Progress of Theoretical and Experimental Physics* **2020**, 083C01 (2020).
 - [33] T. D. Lee and C. N. Yang, *Phys. Rev.* **108**, 1645 (1957).
 - [34] J. W. Cronin and O. E. Overseth, *Phys. Rev.* **129**, 1795 (1963).
 - [35] U. Fano, *Rev. Mod. Phys.* **29**, 74 (1957).
 - [36] U. Fano, *Rev. Mod. Phys.* **55**, 855 (1983).
 - [37] G. Benenti and G. Strini, *Int. J. Quant. Info.* **9**, 73 (2011).
 - [38] M. Jacob and G. C. Wick, *Annals of Physics* **7**, 404 (1959).
 - [39] M. Baumgart and B. Tweedie, *J. High Ener. Phys.* **2013**, 1 (2013).
 - [40] H. Chen and R.-G. Ping, *Phys. Rev. D* **102**, 016021 (2020).
 - [41] R. Horodecki, P. Horodecki, and M. Horodecki, *Phys. Lett. A* **200**, 340 (1995).